USE OF DIRECT NUMERICAL SIMULATION TO ASSESS THE PERFORMANCE OF ACOUSTIC DOPPLER TECHNOLOGY CHARACTERIZING TURBULENT FLOWS

Mariano I. Cantero[a], Carlos M. García[b], Leticia Tarrab[b,c] and Kevin Oberg[d]

[a] *University of Illinois at Urbana-Champaign, Urbana, Illinois, and University of Florida, Gainesville, Florida, USA.* mcantero@illinois.edu

[b]*Laboratorio de Hidráulica, Facultad de Ciencias Exactas, Físicas y Naturales., Universidad Nacional de Córdoba, Av. Filloy s/n, Ciudad Universitaria, Córdoba, Argentina.*
cgarcia2mjc@gmail.com;

[c]*Consejo Nacional de Investigaciones Científicas y Técnicas (CONICET), Argentina.*
ltarrab@efn.uncor.edu.

[d]*U.S.Geological Survey, Office of Surface Water, 1201 W. University Ave., Urbana, IL 61801.*
kaoberg@usgs.gov.

Keywords: Direct numerical simulation, Turbulence, Open channel flow, Acoustic Doppler current profilers.

Abstract. This work presents a systematic analysis of the uncertainty associated to spatial and time sampling strategies used to determine flow discharge with acoustic profilers from moving platforms. The study is performed using data sets with high temporal and spatial resolution from direct numerical simulations of turbulent open channel flow. The simulations results are validated with laboratory scale experimental observations previously reported in the literature. A function of the maximum uncertainty as a function of an appropriately defined measurement time is developed and validated with field scale measurements. The results show that the measurement time is as important as the number of transects performed. The findings of this work are useful tools to define the optimal sampling strategies to perform a good characterization of the flow fields using acoustic profilers.

1. INTRODUCTION

Acoustic Doppler technologies, in particular Acoustic Doppler Velocimeters and Acoustic Doppler Current Profilers (ADV and ADCP hereafter, respectively), are worldwide used to determine flow discharge in rivers and channels. The United State Geological Survey (USGS) has intensively used these technologies since the 1990's and has developed through the Office of Surface Water (OSW) technical memorandums and reports to standardize and optimize the use of ADCP on discharge measurements (see for example OSW Technical memorandums 2002.2, 2006.2 and 2006.4). The guidance developed by the OSW (Oberg et al. 2005; Mueller and Wagner 2006) aim at specifying quality-assurance practices to minimize discharge measurements errors and bias. In this context, the evaluation of the uncertainty on discharge measurements of turbulent flows using ADV and ADCP is of primarily importance.

Many factors affect the uncertainty of discharge measurements such as selecting measurement locations, instrument setting, instrument internal data preprocessing strategy, quality of measured data, and spatial and time sampling strategies. For measurements from moving platforms, the recommended spatial and time sampling strategy for normal flow discharge is a minimum of four transects in reciprocal pairs (a transect is a single pass across the stream). The reported discharge is then computed as the average of the transect pair discharges. Although the use of this strategy is a common practice in many countries, there is no sound research suggesting that four transects is the optimal approach for ADCP stream flow measurements (Oberg and Mueller, 2007). New field studies (Oberg and Mueller 2007) suggest that measurement duration (also named exposure time) has a more important role on reducing the uncertainty of the ADCP stream flow measurement than the number of transects. Along the same line of reasoning and also based on field studies, Czuba and Oberg (2008) claim that exposure time is a critical factor in reducing measurement uncertainty.

A systematic analysis of the uncertainty associated to the spatial and time sampling strategy demands high spatial and temporal resolution of the flow field (Garcia et al., 2005). This requirements are difficult to meet in field even laboratory experiments. The use of Direct Numerical Simulation (DNS) thus presents an ideal tool to generate such detailed data set since it solves for all relevant time and length scales present in the flow with no need for turbulence closure schemes. Although DNS can hardly be applied to field scale flows, the levels of turbulence attained at moderate Reynolds number flows where DNS is feasible, are representative of mature turbulent flows and, based on the Reynolds invariance, the results and findings can be extrapolated with some caution to larger Reynolds number.

This work focuses on the analysis of the uncertainties on ADCP discharge measurements generated by the presence of flow turbulence fluctuations. The analysis addresses specifically the relative importance of factors associated to the spatial and time sampling strategy such as the exposure time in each transect, the number of sampled transects, the instrument sampling frequency, the mean flow velocity, the water depth and the river width on the uncertainty of discharge measurements from moving platforms using ADCP. A dimensional analysis is first presented in order to form the relevant dimensionless groups in the analysis. Then, the functional form of the uncertainty as a function of an appropriately defined dimensionless exposure time is found using DNS generated data for turbulent open channel flows. The simulation is performed for a moderate Reynolds number $Re = 9164$ and is validated with experimental results available in the literature. Then, the simulated three-dimensional instantaneous flow field is sampled by approximating the sampling strategies used by ADCP to assess the uncertainty in the measurements of turbulent flow field reported by these instruments. Finally, the functional form obtained is validated using field measurements. A detailed data analysis is performed to select the best set of data used in the validation process.

The findings of this work are useful tools to define the optimal sampling strategies to perform a good characterization of the flow field using ADCP.

2. DIMENSIONAL ANALYSIS

The relative error in ADCP discharge measurements (ε_Q) can be quantified using information related to the total number of sampled transect (N_T), the exposure time for each transect (D), the river depth (H), the river width (B), the mean flow velocity (V) and the instrument sampling frequency (f). Dimensional analysis shows that in this particular problem there are five degree of freedom which can be represented as five dimensionless numbers. The two dimensionless variables ε_Q and N_T form two dimensionless numbers:

$$\pi_1 = \varepsilon_Q, \tag{1}$$
$$\pi_2 = N_T. \tag{2}$$

The three remaining dimensionless numbers are:

$$\pi_3 = \frac{B}{H}, \tag{3}$$

$$\pi_4 = \frac{V \cdot D}{H}, \tag{4}$$

$$\pi_5 = \frac{H \cdot f}{V}. \tag{5}$$

The dimensionless number π_3 represents the number of flow structures of size H along a river cross section. The dimensionless number π_4 can be rewritten as

$$\pi_4 = \frac{V \cdot D}{H} = \frac{D}{H/V} \tag{6}$$

where $T = H/V$ is the characteristic time of advection for the flow structures of size H. Thus π_4 represents the number of flow structures of size H crossed by the moving platform (boat) in a transect. Finally, the dimensionless number π_5 can also be rewritten as

$$\pi_5 = \frac{H \cdot f}{V} = \frac{T}{\Delta t} \tag{7}$$

where $\Delta t = 1/f$ is the sampling time interval between velocity profiles. Thus π_5 represents the ratio between the time scale of the flow turbulence structure of size H and the sampling time interval between velocity profiles.

Based on Buckingham's Pi theorem the relative error in ADCP discharge measurements (ε_Q) can be expressed as:

$$\varepsilon_Q = F\left(N_T, \frac{B}{H}, \frac{V \cdot D}{H}, \frac{H \cdot f}{V} \right). \tag{8}$$

A new functional relation can be obtained by combining the dimensionless numbers π_2, π_3, π_4, and π_5 as: (Streeter and Wylie 1988):

$$\varepsilon_Q = F_1\left(N_T\left(\frac{B}{H}\right)^{-1}\left(\frac{V \cdot D}{H}\right)\left(\frac{H \cdot f}{V}\right) \right) \tag{9}$$

that is

$$\varepsilon_Q = F_1\left(\frac{N_T \cdot D \cdot f}{B/H} \right). \tag{10}$$

The product ($D\,f$) represents the number of sampled velocity profiles in each transects. Thus ε_Q is represented by a function F_1 of the ratio between the total number of sampled profiles in N_T transects ($N_T\,D\,f$) and the number of flow structures of size H along a river cross section (B/H). The final form of function F_1 is first obtained on the basis of data simulated using numerical methods (DNS).

3. MATHEMATICAL AND NUMERICAL MODEL

A horizontal channel is analyzed in which the flow is driven by a uniform mean pressure gradient in the streamwise direction (x). The dimensionless set of equations that govern the flow read

$$\frac{\partial \mathbf{V}}{\partial t} + \mathbf{V} \cdot \nabla \mathbf{V} = \mathbf{G} - \nabla p + \frac{1}{Re_\tau} \nabla^2 \mathbf{V}, \qquad (11)$$

$$\nabla \cdot \mathbf{V} = 0, \qquad (12)$$

where $\mathbf{V}=(u,v.w)=(u_x,u_y,u_z)$ is the velocity vector, p is the dynamic pressure and $\mathbf{G}= (1,0,0)$ is the (negative of the) mean pressure gradient. Dimensionless variables are defined using the shear velocity, $u_*=(\tau_w/\rho)^{1/2}$, as the velocity scale where τ_w is the bottom wall shear stress and ρ is the fluid density; the channel height, H, as the length scale; and the derived scales $T=H/u_*$ for time and $P=\rho u_*^2$ for pressure. The dimensionless number in equation (11) is the Reynolds number defined as $Re_\tau=u_*H/\nu$ where ν is the dynamic viscosity, and for this work $Re_\tau=509$, which gives a bulk Reynolds number $Re =VH/\nu = 9164$.

The governing equations are solved using a de-aliased pseudospectral code (Canuto, et al., 1988). Fourier expansions are employed for the flow variables in the horizontal directions (x and y mean the streamwise and spanwise directions, respectively). In the inhomogeneous vertical direction (z) a Chebyshev expansion is used with Gauss-Lobatto quadrature points. An operator splitting method is used to solve the momentum equation along with the incompressibility condition (see for example Brown et al., 2001). First, an advection-diffusion equation is solved to compute an intermediate velocity field. After this intermediate velocity field is computed, a Poisson equation is solved to compute the pressure field. Finally, a pressure correction step is performed to obtain the final incompressible velocity field. A low-storage mixed third order Runge-Kutta and Crank-Nicolson scheme is used for the temporal discretization of the advection-diffusion terms. More details of the implementation of this numerical scheme can be found in Cortese and Balachandar (1995). Validation of the code can be found in Cantero et al. (2007a) and Cantero et al. (2007b).

The length of the channel is $L_x=2\pi H$, the width is $L_y=2/3\pi H$, and the height is $L_z=H$. The grid resolution used is $N_x=128$ x $N_y=128$ x $N_z=129$ and the non-linear terms are computed in a grid $3N_x/2$ x $3N_y/2$ x N_z in order to prevent aliasing errors. The bottom wall represents a smooth no-slip boundary to the flow and the top wall is a free slip wall. Then, the boundary conditions employed are:

$$\mathbf{V} = 0 \quad \text{at } z = 0, \text{ and} \qquad (13)$$

$$\frac{\partial u}{\partial z} = 0, \frac{\partial v}{\partial z} = 0, \text{ and } w = 0 \text{ at } z = 1. \qquad (14)$$

The dimensionless integration time employed in this work is $T_i\,u_*/H=35.35$ after the flow has achieved a statistically steady state.

The simulated data using DNS is validated comparing vertical profiles of turbulence parameters for an open-channel flow with experimental results (Nezu, 1977 and Nezu and

Nakagawa, 1993), and semi theoretical curves (Nezu and Rodi, 1986, and Nezu and Nakagawa, 1993).

Mean variables profiles are obtained by time-averaging the instantaneous horizontal plane averages. Using the same approach, turbulence parameters profiles are estimated by using information of the time and horizontal plane perturbations from the mean variable.

Figure 1 shows the vertical profiles of mean streamwise dimensionless velocity in plus units ($u^+ = u/u_*$). This figure also includes the law of the wall for open channel flows (Nezu and Nakagawa, 1993):

$$u^+ = \frac{u}{u_*} = z^+ = \frac{zu_*}{v} \tag{15}$$

which is valid for the viscous sublayer ($z^+ < 5$), and

$$u^+ = \frac{1}{\kappa}\ln(z^+) + A \tag{16}$$

which is known as the log-law and it is inherently valid in the wall region ($z/H < 0.2$). Nezu and Rodi (1986) claim that for smooth open channel flow, the von Karman constant (κ) and the integral constant A have the universal values of 0.41 and 5.29, respectively. The observed deviations from the log-law for $z/H > 0.2$ was also accounted by Nezu and Nakagawa (1993) adding a wake function. A very good agreement is observed between the simulated data using DNS and the velocity distributions for each region.
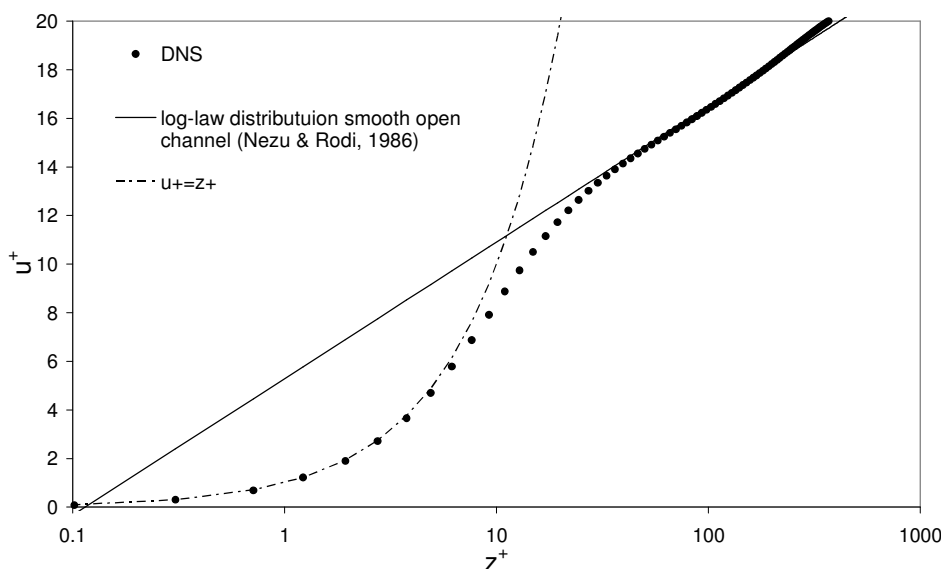
Figure 1: Vertical profile of mean streamwise dimensionless velocity ($u^+ = u/u^*$ and $z^+ = zu^*/v$).

Figures 2, 3 and 4 show vertical profiles of the dimensionless velocity root mean square for the streamwise (u'), spanwise (v') and vertical (w') components, respectively, computed from DNS data. In addition, these figures also include experimental data measured in earlier research work for smooth open channels (Nezu, 1977) and semi-theoretical relations. Semi-theoretical relations for turbulent intensities (equations (17), (18) and (19)), made dimensionless with the shear velocity, were presented by Nezu and Nakagawa (1993) which are valid in the region where the turbulent energy is in equilibrium (the rate of the turbulent energy production is equal to the rate of turbulent dissipation):

$$\frac{u'}{u_*} = D_u \exp\left(-\frac{z}{H}\right) \tag{17}$$

$$\frac{v'}{u_*} = D_v \exp\left(-\frac{z}{H}\right) \tag{18}$$

$$\frac{w'}{u_*} = D_w \exp\left(-\frac{z}{H}\right) \tag{19}$$

where D_u, D_v, and D_w are empirical constants. Hot-film data reported by Nezu (1977) allowed to evaluate these empirical constants as: $D_u = 2.30$, $D_v = 1.63$, and $D_w = 1.27$, which proved to be independent of the Reynolds number and Froude numbers.
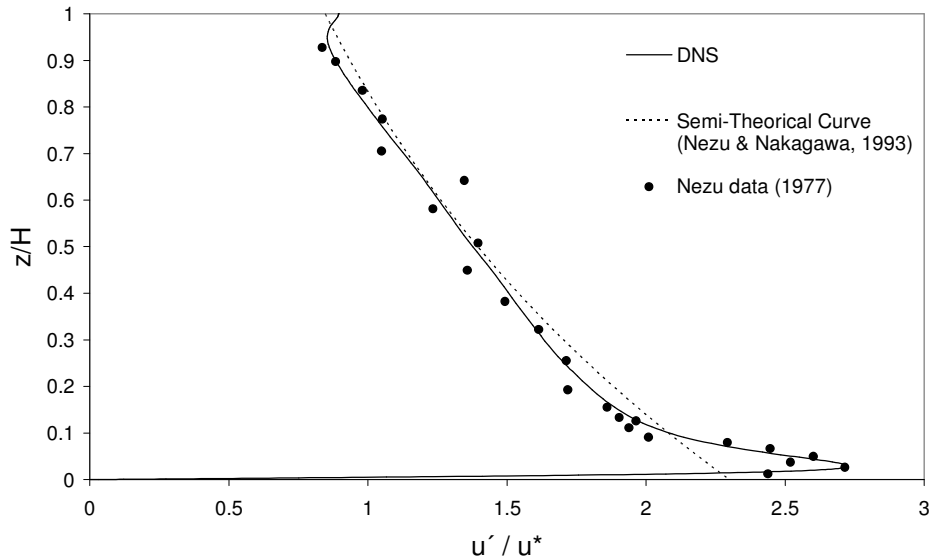
Figure 2: Dimensionless root mean square of water velocity for the streamwise direction (u')
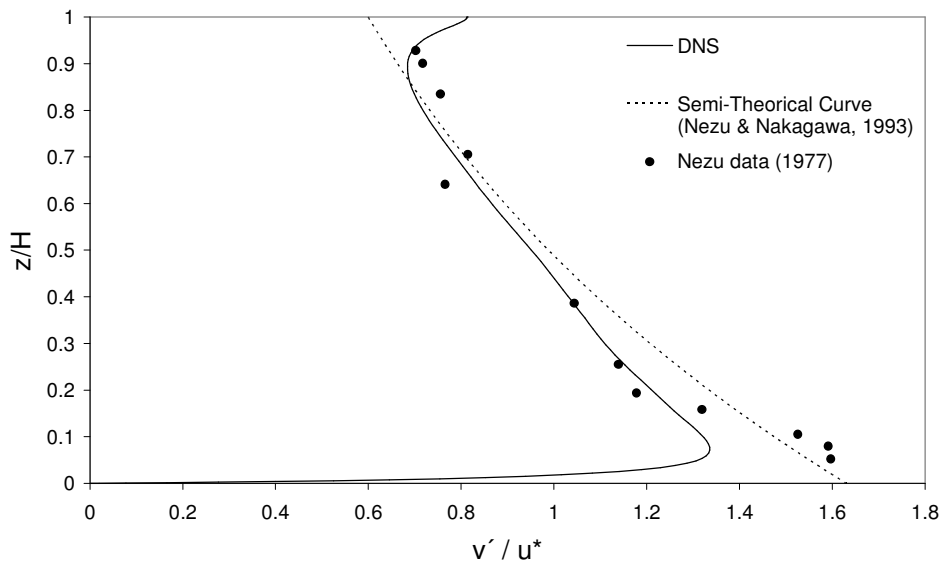
Figure 3: Dimensionless root mean square of water velocity for the spanwise direction (v')

Near the wall $z^+ < 50$, the turbulent generation and dissipation are not in equilibrium. Nezu and Nakagawa (1993) claim that in this region, empirical formulas for the dimensionless root mean square of the water velocity in the streamwise region are more useful for correlating data near the wall. The authors presented the following empirical relation:

$$\frac{u'}{u_*} = 0.3 \cdot z^+ \tag{20}$$

Nezu and Nakagawa (1993) also claim that the distribution of dimensionless root mean square of water velocity for the streamwise direction ($u´$) has a maximum for z^+ = 10 - 20. Figure 5 shows the vertical profile of dimensionless velocity root mean square for the streamwise direction ($u´$) in the region where z/H < 0.4. DNS data shows a good agreement with both equation (20) in the near wall region and Nezu and Nakagawa (1993) estimation of the location of the maximum.

Figure 6 shows a comparison between the vertical profiles of dimensionless turbulent kinetic energy (TKE) computed from DNS data and the semi-theoretical relation proposed by Nezu and Nakagawa (1993) for the region where the turbulent energy is in equilibrium:

$$\frac{TKE}{u_*^2} = D\exp\left(-2\frac{z}{H}\right) \tag{21}$$

Hot-film data reported by Nezu (1977) allowed to evaluate the empirical constant as D = 4.78.
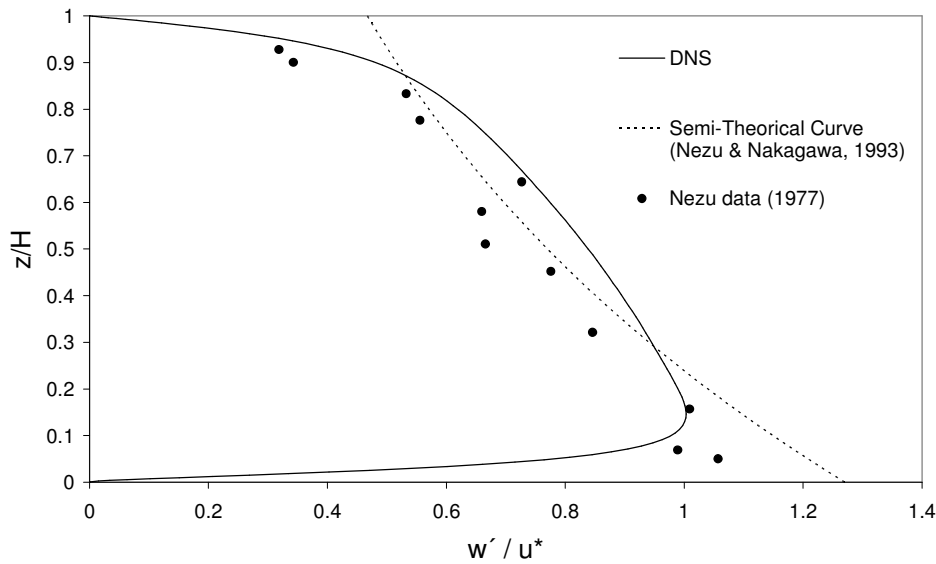
Figure 4: Dimensionless root mean square of water velocity for the vertical direction (w´)
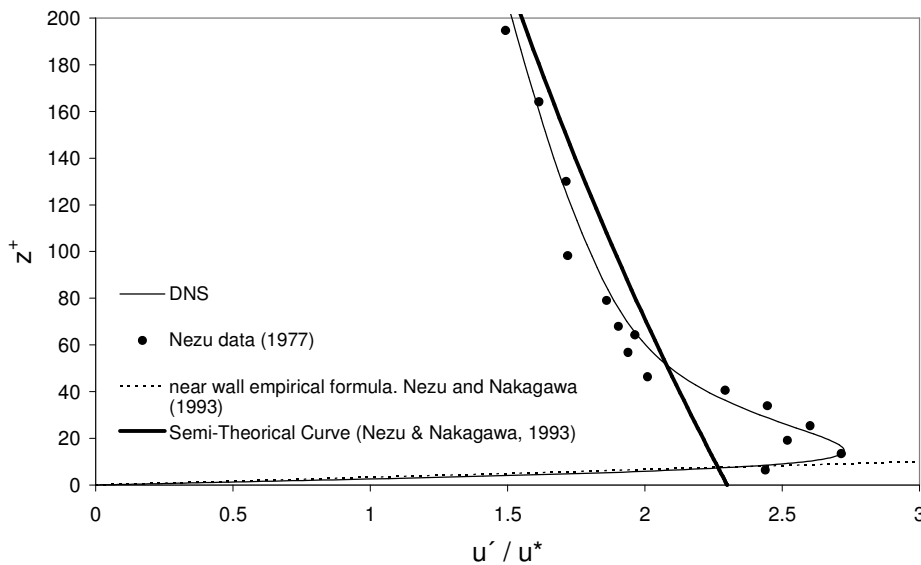
Figure 5: Dimensionless root mean square of water velocity for the streamwise direction ($u´$) in the region z/H < 0.4.
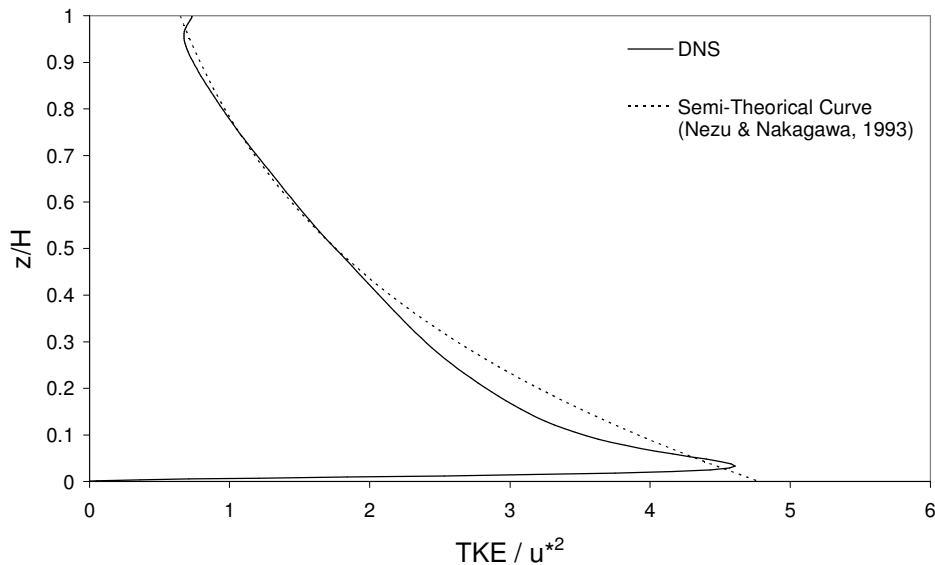
Figure 6: Dimensionless turbulent kinetic energy.

4. FUNCTIONAL FORM OBTAINED FROM DATA SIMULATED USING DNS

First, the form of function F_1 (equation (10)) is obtained on the basis of data simulated using DNS. The flow discharge is computed integrating in the cross section, the high temporal and spatial resolution velocity data generated in the numerical experiments. Then, the synthetic data is sampled at different verticals from a moving platform instrument (simulating ADCP deployment). The main parameters to be varied in the sampling strategy are: the total number of sampled transect (N_T), the exposure time for each transect (D) and the instrument sampling frequency (f).

Variation in measured discharge for a defined same sampling condition can occur because of random error in the instrument, flow turbulence, and unsteadiness of the flow. Only random uncertainty of discharge measurements due to flow turbulence can be analyzed using data generated by DNS. Twelve transects of synthetic water velocity data were sampled for each sampling conditions. The mean discharge from 12 transects is assumed to be the true discharge for the purpose of assessing the uncertainty (or relative error) associated with flow turbulence.

The relative error in discharge measurements (ε_Q) associated with 1, 2, and 4 transects were computed as the percent deviation from the mean of 12 transects (e.g. for N_T =12, ε_Q = 0%). For N_T = 1, 2 and 4, a set of 12, 11 and 9 running means were computed, respectively, using sequential data because multiple transects would be measured sequentially. Thus a set of 12, 11 and 9 different values of ε_Q are available for N_T = 1, 2 and 4, respectively. The maximum relative error in discharge measurements for different numbers of transects and sampling conditions are shown in Figure 7. The values included in this plot are computed varying the total number of sampled transect (N_T) and the exposure time for each transect (D) while f and the ratio H/B remain fixed. As expected, the maximum relative error in discharge measurement decreases as the exposure time increases. This figure also shows that a similar value of maximum relative error in discharge measurements (ε_Q) can be achieved by either varying N_T or D. Finally, Figure 7 includes the best fit curve (R^2 = 0.88) of all the simulated data:

$$\varepsilon_{Q_{\max}} = 3.73\left(N\ D\ f\ \frac{H}{B} \right)^{-0.38} \tag{22}$$
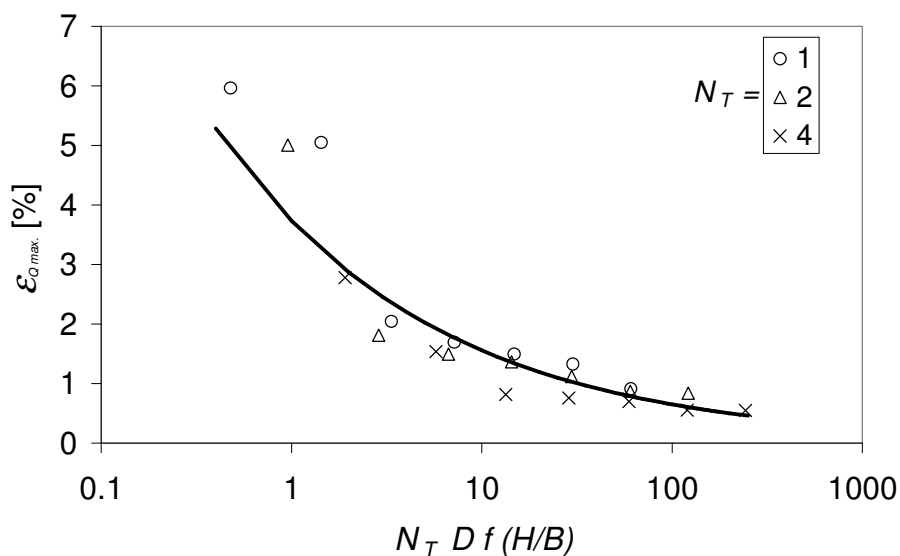
Figure 7: Maximum relative discharge estimate ($\varepsilon_{Q\ max}$) as a function of the dimensionless exposure time.
The solid line represents the best fit indicated in equation (22).

5. FUNCTIONAL FORM OBTAINED FROM DATA RECORDED DURING FIELD MEASUREMENTS

Finally, the functional form obtained using DNS data (equation (22)) is validated using field data which presents aspect ratio (H/B) values different from the conditions simulated using DNS. Due to the fact that only random uncertainty of discharge measurements due to flow turbulence can be analyzed using DNS data, a detailed data analysis is performed to select the best set of available data to be used in the validation process (i.e. noise effects are not included). Table 1 presents the sites chosen for this study.

Table 1: Description of the sites chosen for this study.

Site ID	Station No	Station Name	Latitude	Longitude	Drainage Area [km^2]
Algonquin	05550000	Fox River at Algonquin, Illinois	42.166	−88.290	3,630
Burlington	07182510	Neosho River at Burlington, Kansas	38.195	−95.735	7,880
Chester	07020500	Mississippi River at Chester, Illinois	37.904	−89.836	1,840,000
Dunns	05517500	Kankakee River at Dunns Bridge, Indiana	41.219	−86.969	3,500

The measurements selected for the validation of the functional form obtained using DNS present a variety of flow and sampling conditions. Table 2 summarizes the main parameters describing the measuring conditions for each data set. Each data set included in Table 2 consists of velocity data recorded during 12 transects.

Every selected set of field data (12 transects each) described in Table 2 is analyzed with the same methodology used for DNS. Also, the mean discharge from 12 transects is assumed to be the true discharge. The relative error in discharge measurements (ε_Q) associated with 1, 2, and 4 number of transects were computed as the percent deviation from the mean of 12 transects (e.g. for N_T =12, ε_Q = 0%).

Figure 8 shows the maximum relative error in discharge measurements for the data sets Chester 1 and Chester 2 which present the best data quality (see table 3). This figure also includes all the data and the best fit from DNS.

Table 2: Description of the sites chosen for this study.

| Data set | Instrument configuration | | Disch. Q [m³/s] | River Width [m] | Mean Flow Velocity [m/s] | Average Exposure Time for 1 Transect. [seconds] | Mean Boat Velocity [m/s] | Average Number of Profiles for 1 Transect | Mean Water Depth [m] |
	Freq. [KHz]	Water Mode							
Chester 1	600	1	3270	487.6	1.08	497	1.01	807	6.19
Chester 2	600	1	3243	486.3	1.08	476	1.08	773	6.17
Burlington 1	1200	12	142.2	36.7	1.40	158	0.24	110	2.76
Burlington 2	1200	12	141.9	37.0	1.49	78	0.48	202	2.57
Dunns 2	1200	5	23.5	29.9	0.49	145	0.21	242	1.61
Algonquin	600	11	36.7	105.0	0.14	268	0.40	394	2.42

Table 3 summarize some of the main parameters characterizing the quality of every data set analyzed in this study.

Table 3: Parameters characterizing the quality for every data set

Data Set	Average Ratio between Measured Q and Total Q	Maximum Number of Bad Ensembles
Chester 1	71.8%	1
Chester 2	71.4%	2
Burlington 1	69.6%	4
Burlington 2	64.7%	5
Dunns 2	64.9%	13
Fox_AlQ	68.4%	1

Figures 9 and 10 show the maximum relative error in discharge measurements for data sets which present average ratio between measured flow discharge and total flow discharge greater than 65% and 60%, respectively. These figures show that as the quality of the data set decreases, the dispersion of the observed point increases.
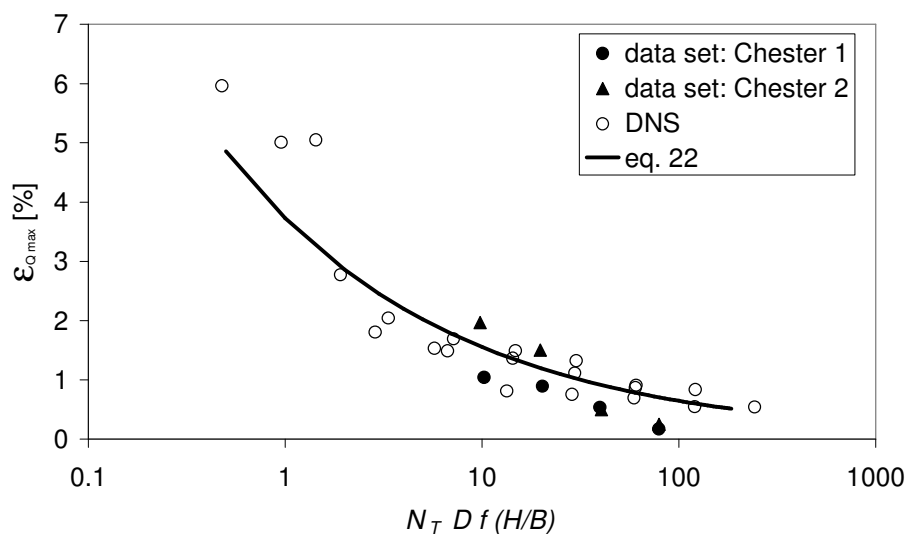
Figure 8: Maximum relative discharge estimate ($\varepsilon_{Q\,max}$) as a function of the dimensionless exposure time estimated from numerical simulation (DNS and eq. 22) and field data (Chester 1 and Chester 2 data set).
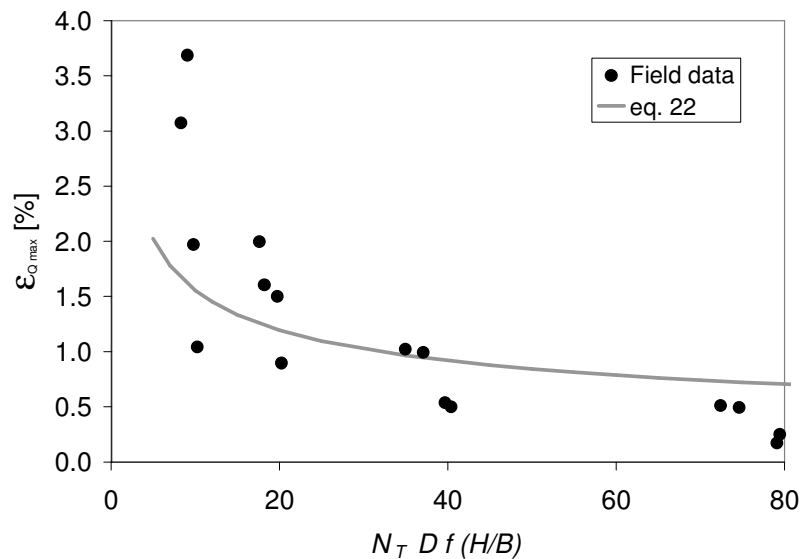
Figure 9: Maximum relative discharge estimate ($\varepsilon_{Q\,max}$) as a function of the dimensionless exposure time estimated from numerical simulation (DNS fitting) and field data sets which present average ratio between measured flow discharge and total flow discharge greater than 65%.
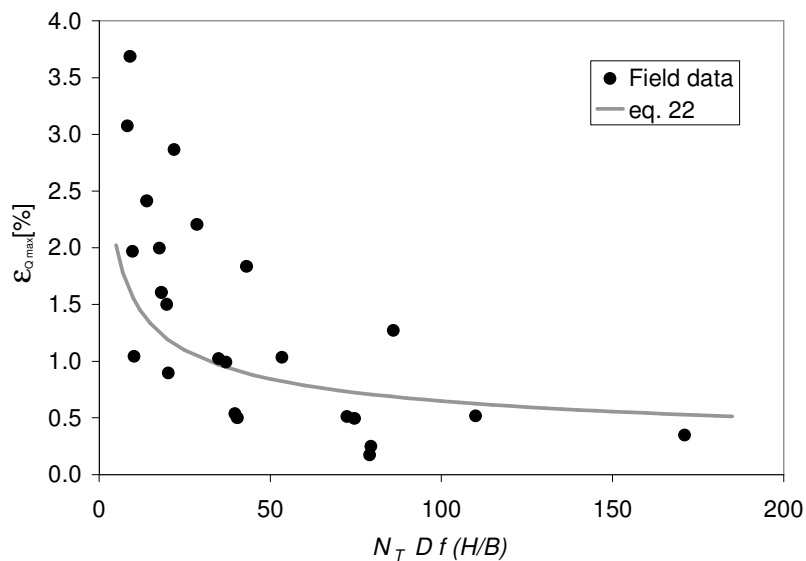
Figure 10: Maximum relative discharge estimate ($\varepsilon_{Q\,max}$) as a function of the dimensionless exposure time estimated from numerical simulation (DNS fitting) and field data sets which present average ratio between measured flow discharge and total flow discharge greater than 60%.

6. CONCLUSIONS

A systematic analysis technique for the uncertainty associated to spatial and time sampling strategies in flow discharge measurements with ADCP from moving platforms has been presented. The study is based on a high temporal and spatial resolution date set from DNS of turbulent open channel flow at moderate Reynolds numbers. The levels of turbulence attained in the simulation presented in this work can be considered as representative of mature turbulent flows as shown from the comparison with experimental results reported in the literature. Based on the Reynolds invariance, the results and findings can be extrapolated with some caution to larger Reynolds number.

The main finding of the work is the development of a functional relation between the maximum uncertainty in discharge measurement and an appropriately defined measurement time. The functional relation has been compared to field scale measurements showing very good agreement. Based on the work findings it can be concluded that the measurement time is as important as the number of transects performed. More work in underway at this time aiming at modifying current measurement protocols.

7. ACKNOWLEDGMENTS

DISCLAIMER. Use of trade, product, or firm names in this paper is for descriptive purposes only and does not imply endorsement by the U.S. Government.

8. REFERENCES

Brown, D., Cortez, R., and Minion, M., Accurate Projection Methods for the Incompressible Navier–Stokes Equations. *Journal of Computational Physics*, 168(2):464-499, 2001.

Cantero, M., Lee, J., Balachandar, S., and García, M., On the front velocity of gravity currents. *Journal of Fluid Mechanics*, 586:1-39, 2007a.

Cantero, M., Balachandar, S., and García, M., High resolution simulations of cylindrical density currents. *Journal of Fluid Mechanics*, 590:437-469, 2007b.

Canuto, C., Hussaini, M.Y., Quarteroni, A., and Zang, T.A., *Spectral Methods in Fluid Dynamics*, Springer, New York, U.S.A, 1988.

Cortese, T., and Balachandar,S, High Performance Spectral Simulation of Turbulent Flows in Massively Parallel Machines With Distributed Memory. *International Journal of High Performance Computing Applications*, 9(3):187-204, 1995.

Czuba, J., and Oberg K., Validation of Exposure Time for Discharge Measurements made with Two Bottom-Tracking Acoustic Doppler Current Profilers. 9th Working conference on Current Measurement Technology, IEEE, Charleston, South California, USA, 2008.

García, C., Cantero, M., Niño, Y., and García, M., Turbulence measurements using Acoustic Doppler Velocimeter. *Journal of Hydraulic Engineering*, 131(12):1062-1073, 2005.

Mueller, D., and Wagner C., Application of the Loop Method for Correcting Acoustic Doppler Current Profiler Discharge Measurements Biased by Sediment Transport. U.S. Geological Survey Scientific Investigations Report 2006-5079, 2006.

Nezu, I. *Turbulence structure in open channel flows*. Ph.D Thesis. Kyoto University. Kyoto, Japan, 1977.

Nezu, I., and Nakagawa, H., *Turbulence in open channels*. AA Balkema, Rotterdam, The Netherlands, 1993.

Nezu, I., and Rodi W., Open-Channel Flow Measurements with a Laser Doppler Anemometer. *Journal of Hydraulic Engineering*, 112(5):335-355, 1986.

Oberg, K., Morlock, S., and Caldwell, W., Quality-Assurance Plan for Discharge Measurements Using Acoustic Doppler Current Profilers. U.S. Geological Survey Scientific Investigations Report 2005-5183, 2005.

Oberg, K., and Mueller, D., Validation of Streamflow Measurements Made with Acoustic Doppler Current Profilers. *Journal of Hydraulic Engineering*, 133(12):1421 – 1432, 2007.

Streeter V., and Wylie B., *Fluid Mechanics*. 8th Edition. McGraw-Hill Inc. USA, 1988.